Dynamic Complex Liquid Crystal Emulsions

Dynamic Complex Liquid Crystal Emulsions

Alberto Concellón, Cassandra A. Zentner, and Timothy M. Swager*

Department of Chemistry, Massachusetts Institute of Technology, 77 Massachusetts Avenue, Cambridge, Massachusetts 02139, United States.

ABSTRACT: We report a new class of dynamically reconfigurable complex colloids comprising immiscible liquid crystals (LCs) and fluorocarbon oils. Producing stable spherical droplets requires the utilization of appropriately designed surfactants to reduce the high intrinsic surface tension between the LCs and the fluorocarbon oils that initially lead to non-spherical, "snowman-shaped" Janus droplets. After stabilizing the interfaces *via* surfactants, the LC droplet morphology can be dynamically switch between LC-in-fluorocarbon-in-water double emulsions (LC/F/W), spherical Janus emulsions, and inverted double emulsions (fluorocarbon-in-LC-in-water, F/LC/W) in response to changes in the surrounding surfactants. These stabilization methods can be extended to smectic LCs to create droplets with more complex internal arrangements and expand the range of LC emulsions that can be prepared. In addition, by using new mesogenic surfactants that control the LC director field at each LC-interface, we prepare LC complex colloids exhibiting different internal configurations. The ability to control the LC anchoring conditions made possible to create topological singularities as powerful templates for the precision assembly of antibodies at the droplets' interface. These dynamic LC complex colloids of controllable morphology and LC orientation are rich soft materials platforms that will find utility in a variety of sensing applications.

INTRODUCTION

Complex multi-phase liquid emulsions are of increasing importance for real-world applications in pharmaceutical formulations, medical diagnostics, microcapsule fabrication for drug delivery, chemical sensing, and food enhancement.[1-5] Precision colloidal droplets provides rich and fascinating properties and functions that are related to their geometry and composition,[5-6] and microfluidics enable the fabrication of highly sophisticated complex emulsions with precise control of size and internal structure.[7-8] In this context, our group has recently described an effective one-step approach for the preparation of complex emulsion droplets with highly controllable and reconfigurable morphologies.[9] These complex colloids were produced by dispersing a single organic/fluorocarbon phase at elevated temperatures in an aqueous continuous phase that contains surfactants and phase separation of the oils occurs upon cooling. Optical changes caused by surfactant or analyte triggered changes in droplets' morphology or alignment have demonstrated utility for the detection biomolecules or pathogens.[10-14] Additionally, the dynamic optical properties of these complex colloids have utility as imaging elements wherein micro-lens arrays can be used to project or capture real or virtual images and display variable focal lengths.[15]

Colloidal solutions with increasing complex internal organizations can ultimately enable new untapped opportunities, and to this end we are interested in creating colloids containing nanostructured fluids, such as liquid crystals (LCs). LCs are a fascinating class of anisotropic soft materials that are capable of self-assembling over length scales from molecular to macroscopic and display collective behavior.[16-17] These are the enabling features for the applications of LCs in optics, sensors, or actuators.[18-19] Colloidal particles of nematic LC fluids have been investigated intensively and methods to control the internal configuration of the LC molecules (mesogens) as well as the colloidal shape have been reported.[20-21] Recent studies have further demonstrated that lipids, surfactants, proteins, or viruses adsorbed at the aqueous interface change the LC orientational order to enable sensitive sensor technologies.[22-24] The spherical confinement of LCs into droplets or shells also constitutes a stimulating tool in soft matter and applications including cholesteric LC emulsion photonic elements,[25-29] and soft actuators based on LC networks.[30-33] Most LC colloids are single emulsion droplets or shells surrounded by inner and aqueous phases with only a few studies of complex LC emulsions.[34-35]

Herein, we describe LC complex colloids where one component is a LC and the other is an isotropic fluorocarbon oil, and demonstrate how the anisotropic nature of the LC compartment can introduce new functionalities and unusual behaviors. The substitution of isotropic hydrocarbon oils by LCs results in a destabilization of the internal interface with the fluorocarbon phase thereby leading to the formation of non-spherical double emulsions. As a result, we report new methods to decrease these internal interfacial tensions needed to stabilize spherical structures over the

range of droplet morphologies: LC-in-fluorocarbon-in-water double emulsions (LC/F/W), Janus emulsions, and inverted double emulsions (fluorocarbon-in-LC-in-water, F/LC/W). We also report new mesogenic surfactants for creating LC complex colloids exhibiting different internal configurations. The ability to control the anchoring and interfacial tension at each LC-interface enable defined configurations with thermodynamically stable defects of varied topologies. We demonstrate that LC generated topological defects are powerful templates for the spatial organization of biomolecules at the droplets' interface for future biological and sensing technologies.

RESULTS AND DISCUSSION

Preparation of LC Double Emulsions. To produce dynamic multicompartment emulsions containing LCs, we chose the nematic LC 4-cyano-4'-pentylbiphenyl (5CB) (thermal transitions: Cr 24 N 35 I) for the hydrocarbon phase and hydrofluoroethers (HFEs) as the fluorocarbon phase. Our temperature-induced phase separation process to create droplets is limited to materials with easily accessible upper critical temperatures (T_c).[9] Unfortunately, the T_c of 5CB/HFE mixtures are outside of convenient temperature ranges. Therefore, we have utilized an evaporation-induced phase separation method.[36-37] Two immiscible fluids (5CB and HFEs) generate a homogenous mixture with the addition of dichloromethane (DCM). In a typical preparation, we emulsified a 1:1:2 volume ratio of 5CB/HFEs/DCM in an aqueous solution containing 0.1 wt. % of the nonionic surfactant Tween-20. After complete evaporation of DCM, "snowman-shaped" Janus droplets with two phase-separated compartments are formed (Figure 1a). The morphology of these complex emulsions of two immiscible liquids F and LC in a third immiscible liquid W is exclusively controlled by the relative interfacial tensions between LC-W (γ_{LC}), F-W (γ_F), and LC-F ($\gamma_{LC/F}$). These three interfacial tensions determine the equilibrium droplet configuration (Figure 1b), which can be characterized by the contact angles between γ_{LC} and $\gamma_{LC/F}$ (θ_{LC}) and between γ_F and $\gamma_{LC/F}$ (θ_F) at the junction point (where the three phases came into contact).[38] Note that we assumed that the orientational order and elasticity of the LC molecules don't substantially affect the three-phase boundary.[34] This balance of forces can be expressed by the following equations:

$$\cos(\theta_{LC}) = \frac{\gamma_F^2 - \gamma_{LC}^2 - \gamma_{LC/F}^2}{2 \cdot \gamma_{LC/F} \cdot \gamma_F}$$

$$\cos(\theta_F) = \frac{\gamma_{LC}^2 - \gamma_F^2 - \gamma_{LC/F}^2}{2 \cdot \gamma_{LC/F} \cdot \gamma_F}$$

When $\gamma_{LC/F}$ is significantly smaller than γ_{LC} and γ_F, droplets adopt spherical shapes and slight changes in the balance of interfacial tensions with the water induce dramatic changes in the droplet morphology.[9] However, as $\gamma_{LC/F}$ increases, droplets seek to minimize LC-F interfacial area and become "snowman-shaped".[39] We explored this relationship by comparing the morphology of double emulsions comprising 5CB and varying HFE oils and the corresponding $\gamma_{LC/F}$ (Table S1). In agreement with above equations, as $\gamma_{LC/F}$ decreased gradually from 7.67 to 4.44 mN/m, Janus droplets exhibited an increased LC-F surface area (Figure 1a). All further studies were performed using HFE7200 as fluorocarbon phase to achieve near-spherical morphology as a result of the lower $\gamma_{LC/F}$ with LC phases.

Bulk emulsification leads to polydisperse droplet sizes (Figure S1), but it enables rapid fabrication with standard laboratory equipment and provides droplets with highly uniform morphology and composition. The evaporation-driven phase separation route is also compatible with microfluidic routes to monodisperse complex LC colloids on a large scale (Figure 1d).

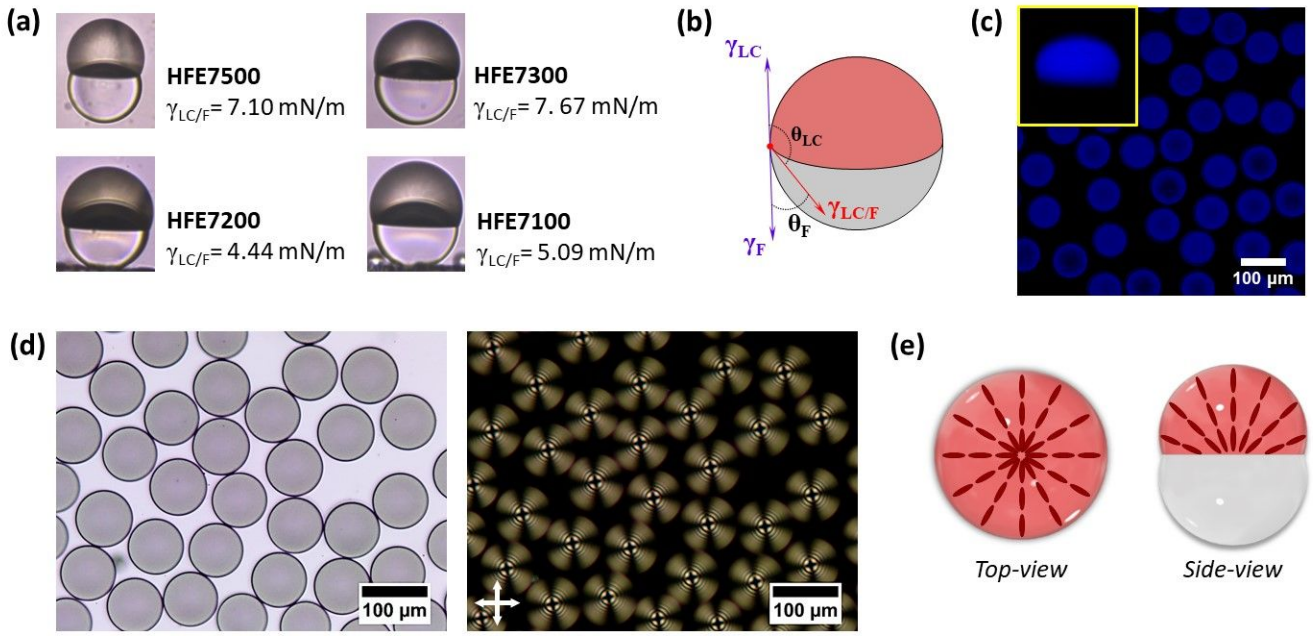

Figure 1. Characterization of the Janus "snowman-shaped" droplets: **(a)** Side-view microscope images and $\gamma_{LC/F}$ interfacial tension varying the fluorocarbon phase. **(b)** Schematic representation of interfacial tensions of a Janus droplet. **(c)** Confocal microscopy images (inset: side-view 3D visualization of the LC compartment). **(d)** Polarized-light optical microscopy images without (left) and with (right) crossed polarizers. **(e)** Schematic representation of radial alignment.

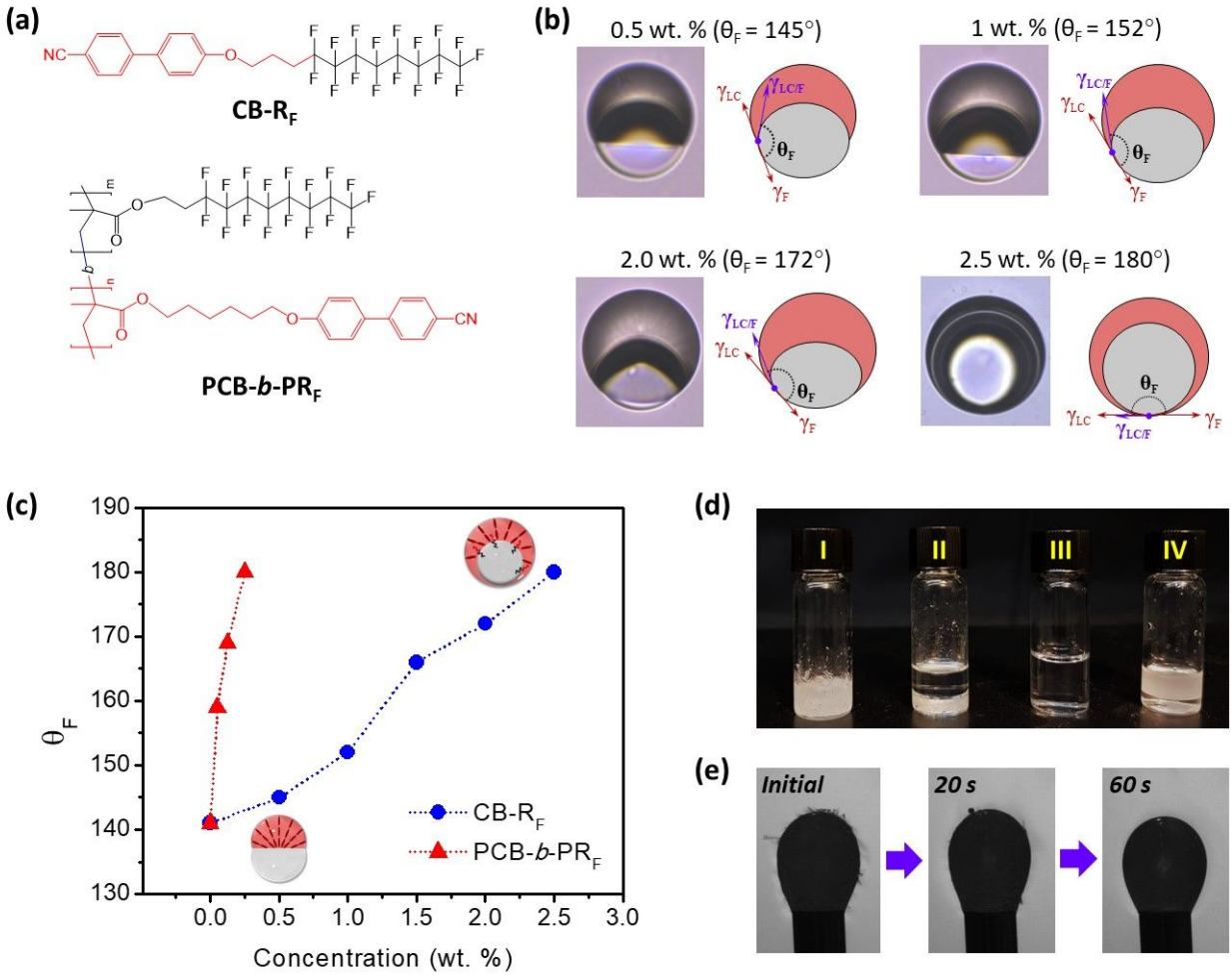

Figure 2. LC/F interface internal surfactant: **(a)** Chemical structure of the LC/F internal surfactants. **(b)** Side-view microscope images varying **CB-R$_F$** concentration and the corresponding sketch of the interfacial tensions (the blue and red lines represent the direction of the three interfacial tensions while their lengths are arbitrary; all droplets were prepared in a 0.1 wt. % aqueous solution of Tween-20). **(c)** θ_F *vs* concentration of internal LC/W surfactant (the values reported for θ_F were averaged of at least 5 independent measurements; a 0.1 wt. % aqueous solution of Tween-20 was used as the continuous phase). **(d) CB-R$_F$** solubility in 5CB and HFE7200: I) Mixture of **CB-R$_F$** (2.5 wt. %) in 5CB, II) Mixture of **CB-R$_F$** (2.5 wt. %) in 5CB after addition of HFE7200, III) Mixture of **CB-R$_F$** (2.5 wt. %) in 5CB and HFE7200 using DCM as cosolvent, and IV) Mixture of **CB-R$_F$** (2.5 wt. %) in 5CB and HFE7200 after DCM evaporation. **(e)** Snapshots showing the evolution of a droplet with dissolving and partitioning of surfactant. Deformation at the interface in initial and 20 s images is due to surfactant particulates before partitioning and alignment at the LC-F interface.

Polarized-light optical microscopy (POM) of these colloids reveal that the optically isotropic fluorocarbon appeared dark, while birefringent LC appeared bright with an extinction point at the center of the droplets (Maltese cross texture) (Figure 1d). These POM textures are indicative of a radial configuration in which the LC molecules anchor perpendicular to the aqueous phase (Figure 1e and Figure S2a). Using a confocal laser scanning microscope, we were able to further characterize their morphology in 3D (Figure 1c inset). Upon addition of perylene to the mixture, bright blue fluorescence was observed only from the top hemisphere, indicating that this dye selectively partitions into the LC phase.

Stabilization of LC Double Emulsions *via* Internal Surfactant. Although our "snowman-shaped" Janus droplets are stable with balanced interfacial tensions, perfect spherical morphologies were not realized as a result of a significant $\gamma_{LC/F}$. We hypothesized that the $\gamma_{LC/F}$ can be reduced to produce perfect spheres by the addition of an appropriately designed internal surfactant. Accordingly, we synthesized monomeric and polymeric surfactants containing a LC and F components designed to organize at the internal interface (Figure 2a).

All the internal surfactants were dissolved in the 5CB/HFE7200/DCM solution which was then emulsified in a 0.1 wt. % aqueous solution of Tween-20. After DCM evaporation, stable Janus droplets were obtained with **CB-R$_F$** and **PCB-*b*-PR$_F$** internal surfactants. Figure 2b reveals that the interfacial area between the LC and F phases expands with increasing the **CB-R$_F$** concentration, demonstrating a lowering of $\gamma_{LC/F}$. To better demonstrate this phenomenon quantitatively, we performed numerical analysis on the topology of the Janus droplets prepared in 0.1 wt. % Tween-20 in order to characterize how close a droplet is to a symmetrical Janus droplet.[40] The equilibrium shape of droplets is fully determined by the contact angles between the interfaces which are used to calculate interfacial tensions.[38] Since LC/F surfactant molecules exclusively concentrate at the internal interface, γ_{LC} and γ_F remain constant; changes in θ_F are controlled by $\gamma_{LC/F}$. Accordingly, we used θ_F to estimate the distortions from a perfect spherical Janus droplet and θ_F is 90° in the symmetrical (spherical) Janus state, 0° in a 5CB-in-HFE7200-in-water (LC/F/W) double emulsion, and 180° in a HFE7200-in-5CB-in-water (F/LC/W) double emulsion.[40] An example of the analysis is shown in Figure 2b wherein the junction point was first determined, and then angles between three tangential lines were drawn. θ_F increases with increasing concentration of **CB-R$_F$** and **PCB-*b*-PR$_F$**, as a result of their localization at the LC/F interface. At a concentration of 2.5 wt. % **CB-R$_F$** or 0.25 wt. % **PCB-*b*-PR$_F$**, emulsification in 0.1 wt. % Tween-20 generated droplets that adopt a spherical F/LC/W double emulsion configuration (θ_F= 180°), which is the expected morphology with sufficiently low $\gamma_{LC/F}$ and Tween-20.

The $\gamma_{LC/F}$ values can be determined at different concentrations of **CB-R$_F$** and **PCB-*b*-PR$_F$** independently by pendant drop analysis (Table S1 and Figure 2e). To this end, LC solutions were prepared by mixing the corresponding LC/F surfactant, 5CB, and DCM. DCM was evaporated overnight, the resulting mixture was heated above the LC clearing point, and pendant drop measurements were made in HFE7200. The pendant drop measurements support the θ_F calculations, where $\gamma_{LC/F}$ decreases from 4.0 to 3.2 mN/m with increasing concentration of **PCB-*b*-PR$_F$** from 0.05 to 0.25 wt. %. Further, at higher concentrations of **PCB-*b*-PR$_F$** the pendant drops become unstable overtime, which is related to a great decrease in $\gamma_{LC/F}$ below measurement capabilities.

At high wt. % of **CB-R$_F$** (> 1 wt %) a viscous heterogeneous mixture with 5CB was obtained (Figure 2d, vial I), and after the addition of HFE7200, **CB-R$_F$** was still not solubilized in this biphasic mixture (Figure 2d, vial II). However, the addition of DCM generates a homogeneous solution (Figure 2d, vial III) and after overnight evaporation of DCM a homogeneous biphasic mixture is generated (Figure 2d, vial IV). These observations suggest that the LC/F surfactants are as expected only partially soluble in both phases and localize at the LC/F interface after DCM evaporation. The partitioning of **CB-R$_F$** is further demonstrated in pendant drop measurements, wherein deformation along the LC/F interface is observed (Figure 2e). Initially, the **CB-R$_F$** is in particulate form and the time profile in Figure 2e shows that the particles dissolve at the interface with HFE7200 to produce an equilibrium $\gamma_{LC/F}$ (Figure 2e). As a result of complexities in solubility of **CB-R$_F$**, the interfacial tension appears to display an abnormal increase until equilibrium reached (Figure S3). With the addition of 0.5 wt. % of **CB-R$_F$** a $\gamma_{LC/F}$ = 4.28 mN/m was obtained. This decrease in $\gamma_{LC/F}$ is small relative to that produced by **PCB-*b*-PR$_F$** at a 10 times lower concentration, thereby demonstrating the higher performance of the polymeric surfactant. All of the pendant droplet results are in good agreement with θ_F measured directly in the complex emulsions.

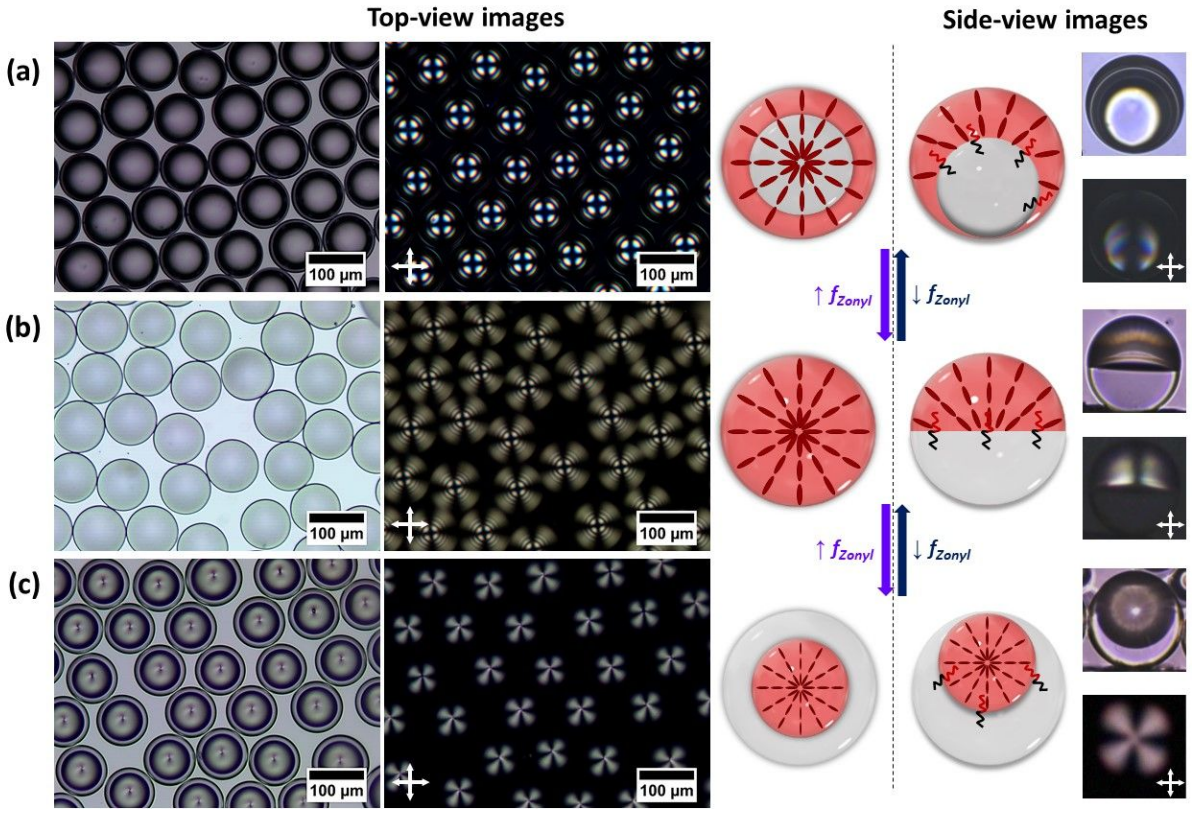

Figure 3. Complex emulsions with a radial alignment of the LC molecules: polarized-light optical microscopy images without (left) and with (right) crossed polarizers of 5CB-HFE7200 droplets that reconfigure in response to variation in the mass ratio of hydrocarbon and fluorocarbon surfactants (f_{Zonyl}): **(a)** F/LC/W double emulsions (f_{Zonyl} = 0–0.15), **(b)** spherical Janus droplets (f_{Zonyl} = 0.20–0.35), and **(c)** LC/F/W double emulsions (f_{Zonyl} = 0.4–1).

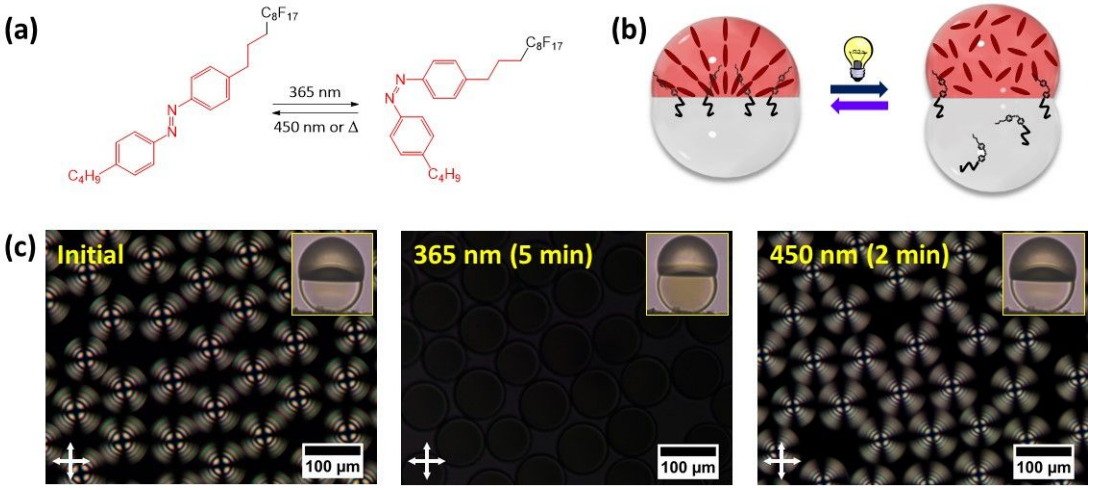

Figure 4. Light-responsive LC/F internal surfactant: **(a)** Chemical structure of the light-responsive internal surfactant (**AZO-R_F**) which reversibly isomerizes under UV irradiation between the rod-like *trans* form of the surfactant and the bent-shaped *cis* form. **(b)** Schematic representation of Janus droplets containing **AZO-R_F** in which UV light irradiation results in a disorder of the nematic LC phase. **(c)** Polarized-light optical microscopy images of the photoinduced phase transition from nematic to isotropic upon irradiation at 365 nm, and subsequent phase transition from isotropic to nematic upon 450 nm irradiation (inset: corresponding side-view images).

Having reduced the $\gamma_{LC/F}$, dynamic reconfiguration of the double emulsions is readily achieved in LC/F droplets through changes in hydrocarbon/fluorocarbon surfactant mass balance.[9] Consequently, emulsification of a 1:1:2

volume ratio of 5CB/HFE7200/DCM with 2.5 wt. % **CB-R_F** or 0.25 wt. % **PCB-*b*-PR_F** in a 0.1 wt. % aqueous solution of Tween-20, generated a spherical F/LC/W double emulsion after complete evaporation of DCM (**Figure 3a**). Gradual introduction of the nonionic fluorosurfactant Zonyl FS-300 (thereafter Zonyl), the droplet morphology dynamically changed passing through a spherical Janus morphology (Figure 3b) before inverting to LC/F/W double emulsion (Figure 3c). The droplets morphology changes were also observed by POM to elucidate the LC ordering throughout the geometry changes. The **CB-R_F** and **PCB-*b*-PR_F** internal surfactants do not impact the normal perpendicular anchoring of 5CB at the fluorous interface (Figure S2b) and both Janus and F/LC/W droplets exhibited radial configurations. In LC/F/W double emulsions the point defect at the center of spherical of the LC compartment confirms a uniform radial anchoring.

Photoswitchable surfactants have been observed to control the LC order at fluid interfaces.[41] Accordingly, we synthesized a light-responsive LC/F surfactant consisting of an azobenzene moiety functionalized with hydrocarbon and fluorocarbon chains (**AZO-R_F** in Figure 4a) to see if dynamic changes at the internal interface could affect the morphology or LC anchoring in complex droplets. When this internal surfactant was used instead of **CB-R_F**, we observed that the Janus droplets rapidly and reversibly change their morphology between a more-spherical to a less-spherical (snowman) Janus droplets in response to UV (λ= 365 nm) and blue (λ= 450 nm) light, respectively. This effect is the result of photoinduced isomerization between the more effective *trans* surfactant the less effective *cis* form (Figure 4, and Video S1). In addition, we observed a distortion of the LC order in response to UV light. With 5 min of UV irradiation the birefringent LC texture disappeared, demonstrating a photoinduced nematic-to-isotropic phase transition. This phase transition is attributed to the *trans*-to-*cis* photoisomerization of **AZO-R_F** as the bent-shaped *cis*-isomers destabilized the order within the mesophase. The same sample was then irradiated with a 450 nm light and the mesophase was recovered within seconds, confirming that the observed photoinduced phase transition was caused by photoisomerization of the azobenzene units and not by local thermal excitation or degradation.

Tuning the Internal Ordering of LC Double Emulsions. The internal organization of LCs confined within micrometer-scale systems is governed by a subtle energetic balance that involves contributions arising from orientation-dependent interfacial energy at the droplet surface, elastic strain associated with deformation of the LC, and the presence of topological defects.[20, 42] Controlling the LC ordering within our complex droplets is central to their utility and can be readily achieved by tuning the surface anchoring of the LC using surfactants.[43] Consequently, we have designed a bolaamphiphilic surfactant, **CB-diTEG** (Figure 5a), which stabilizes the aqueous interface and promotes an alternative planar anchoring of the LC molecules. The surfactant contains a non-polar biphenyl (mesogenic) aromatic core substituted with hydrophilic triethylene glycol groups. The **CB-diTEG** is added to the dispersed phase (containing LC/F internal surfactants) and initially transforms our spherical LC droplets into a monopolar configuration, wherein the mesogens now align parallel (planar) to the LC-W interface and remain perpendicular to the LC-F interface (Figure 5). In addition, a single point defect is localized near the pole of the Janus and F/LC/W droplets. In the case of LC/F/W double emulsions, **CB-diR_F** internal surfactant is used to produce planar alignment at the LC/F interface and produce a bipolar configuration in which two diametrically opposite point defects are present at the poles. Interestingly, a bipolar configuration was also obtained in Janus LC droplets by combining **CB-diTEG** and **CB-diR_F** surfactants. This bipolar configuration exhibits constant LC fluctuation as a result of the fact that the two-point defects are not equatorial poles of the Janus droplets. In this case the defects appear to be localized along the LC/F/W line tension and the defects do not have a thermodynamic anchoring to a specific location (Video S2).

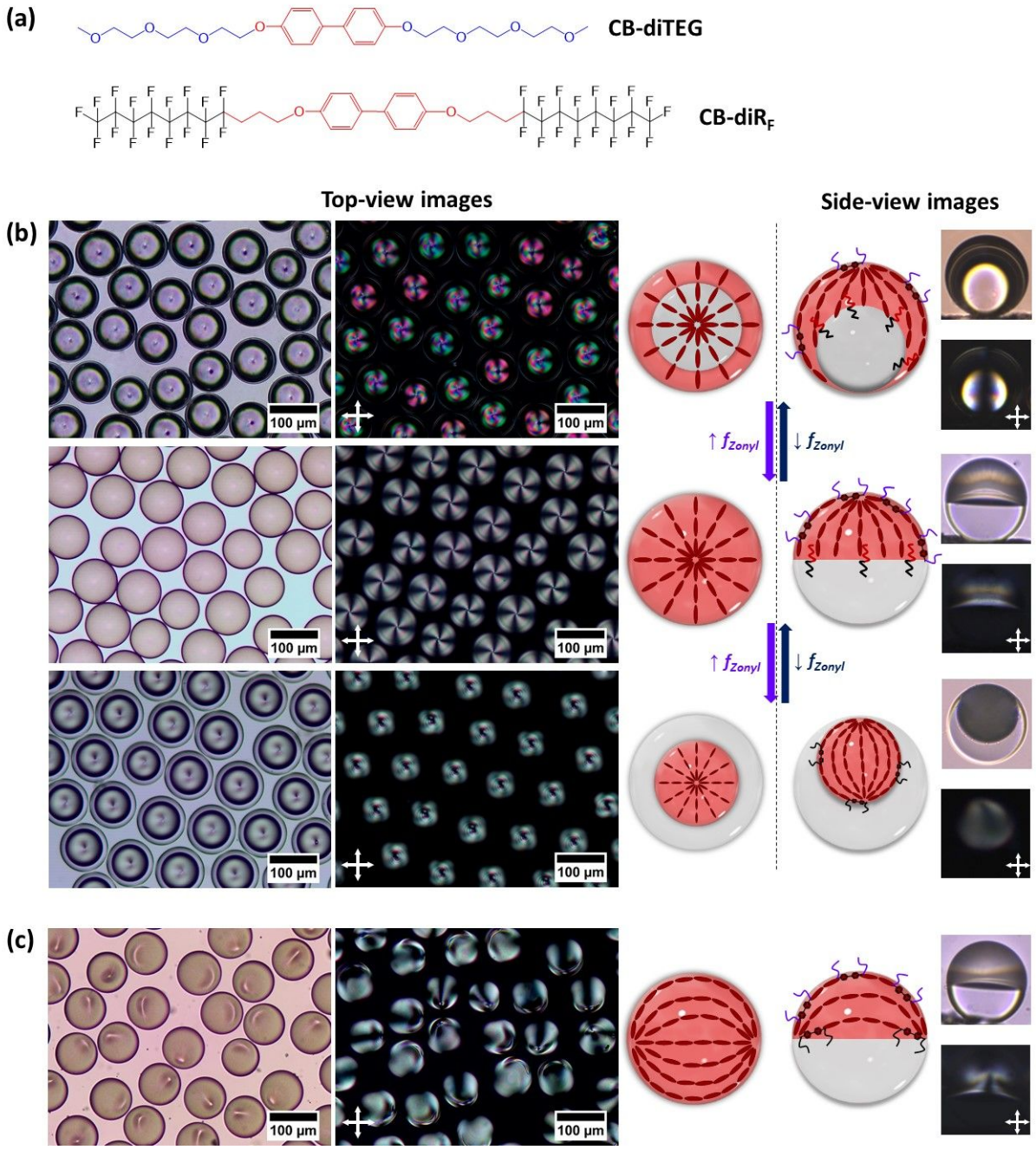

Figure 5. Complex emulsions with a planar alignment of the LC molecules: **(a)** Chemical structures of the surfactants used to induce a planar alignment. **(b)** Polarized-light optical microscopy images of 5CB-HFE7200 droplets which reconfigure in response to surfactant variation: F/LC/W double emulsions in 0.001% Tween-20 (top), spherical Janus droplets in solution of 0.001 wt. % Tween-20 : 0.01 wt. % Zonyl = 3:7 (v:v) (middle), and LC/F/W double emulsions in 0.01 wt. % Zonyl (bottom). **(c)** Bipolar Janus droplets with two points defects moving along a line defined by the LC/F/W three-fold junction (a solution of 0.001 wt. % Tween-20 : 0.01 wt. % Zonyl = 3:7 (v:v) was used as the continuous phase).

LC Double Emulsions with Complex Internal Structure. Emulsions comprising nematic LCs have been extensively studied, however droplets containing smectic phases have seldom been considered.[44-45] The layered structures of smectics affects the defect configuration requiring more complex internal structure within a droplet than those observed for nematics, thereby introducing new possibilities. To this end, we chose to investigate complex droplets with the LC 4-cyano-4'-octylbiphenyl (8CB) which displays a smectic A phase at room temperature and undergoes a phase transition from smectic A (SmA) to nematic (N) at 33°C (*i.e.* Cr 21 SmA 33 N 41 I).

Spherical complex droplets containing 8CB were obtained by using our evaporation-induced phase separation method and internal surfactants to lower $\gamma_{LC/F}$

and obtain spherical droplets. POM images revealed a radial configuration in the initial smectic phase, indicating a perpendicular alignment of the 8CB molecules to the aqueous interface with an extinction point at the center of the droplets (Maltese cross texture) with concentric layers originated from the center of the droplet (Figure 6a). Upon heating the droplets above T_{SmA-N} (33°C), the Maltese cross texture was maintained but the concentric layers disappear, thereby confirming the SmA-to-N transition (Figure 6a). Further heating above 41°C, the isotropic state was reached and LC birefringence disappeared.

The addition of **CB-diTEG** produces SmA droplets with 8CB molecules anchoring parallel to the LC-W interface (planar alignment). When studied by POM, multiple focal-conic defects form a polygonal texture within the LC compartment. This polygonal texture displayed by the SmA LC is the result of half focal-conic domains that pack to fill the half hemispherical space with bases of the cones located at the LC/W interface of the Janus droplet (Figure 6b). With the SmA to N transition at 33°C, we observed a transition from a polygonal texture to a monopolar configuration with a single point defect located at north pole of the Janus droplets. At temperatures above 41 °C, the POM texture again disappeared and the Janus droplets do not have birefringence. The sequence of POM textures of the droplets described above was reversible upon cooling and seen to occur in subsequent heating-cooling cycles. The morphology of these 8CB-HFE7200 droplets can also be dynamically switched between encapsulated (LC/F/W and F/LC/W) and Janus configurations in response to changes in the type and concentration of surrounding surfactants (Figure S4).

Templated Biomolecule Assembly *via* Topological Defect-Driven Functionalization. LC are promising candidates for sensing applications, allowing molecular level events to be observed with the naked eye.[46] The detection principle for most LC sensors relies on highly sensitive orientational responses of LCs to molecular-level perturbations in aliphatic tails caused by foreign molecules adsorbed at LC interfaces.[47] However, expanded methodology for the precision integration of recognition elements is certain to provide additional utility to LC-based sensors for the detection of biomolecules, biomarkers, or organisms. To this end, we have identified the topological defects generated within our LC droplets as powerful sites for bioconjugation because they can act as amplifiers of recognition events, causing dramatic changes in orientation of the LC director fields.

Topological defects in LCs typically assemble around particles that would otherwise disrupt the organization of the phase. The driving force for this process is the minimization of free energy cost associated elastic strain of LCs.[48-51] To determine if we could purposely functionalize these sites, we functionalized the LC/W surface with boronic acid groups that can bind to mono- and polysaccharides and N-glycans present in antibodies. Specifically, we synthesized a block copolymer (**PCB-*b*-PB(OH)$_2$** in Figure 7a) that functions as a cosurfactant in the emulsification process to prepare 5CB-HFE7200 spherical Janus droplets with a monopolar configuration. A low concentration of **PCB-*b*-PB(OH)$_2$** (2.5 mg/mL) maintained the droplets within the Janus configuration and doesn't disrupt the planar surface anchoring provided by **CB-diTEG**. Immobilization of the antibodies at the LC/W interface was accomplished by boronate ester formation between **PCB-*b*-PB(OH)$_2$** and the N-glycans in the Fc-region of the antibody (Figure 7b). Successful functionalization was confirmed by the use of fluoroscein isothiocyanate (FITC) labeled IgG antibodies and imaging by a confocal microscope equipped with crossed polarizers. Combined fluorescent and polarized-light micrographs reveal that the fluorescent signal (the green spots) from surface bound IgG antibodies coincide with the location of the topological defect of the monopolar LC Janus droplets (Figure 7c). Heating IgG-functionalized droplets into an isotropic phase produces a bright fluorescence over the entire LC/W interface (the green fluorescent ring) (Figure 7c). These observations confirm that the polymer bound antibodies selectively localize at the LC defects.

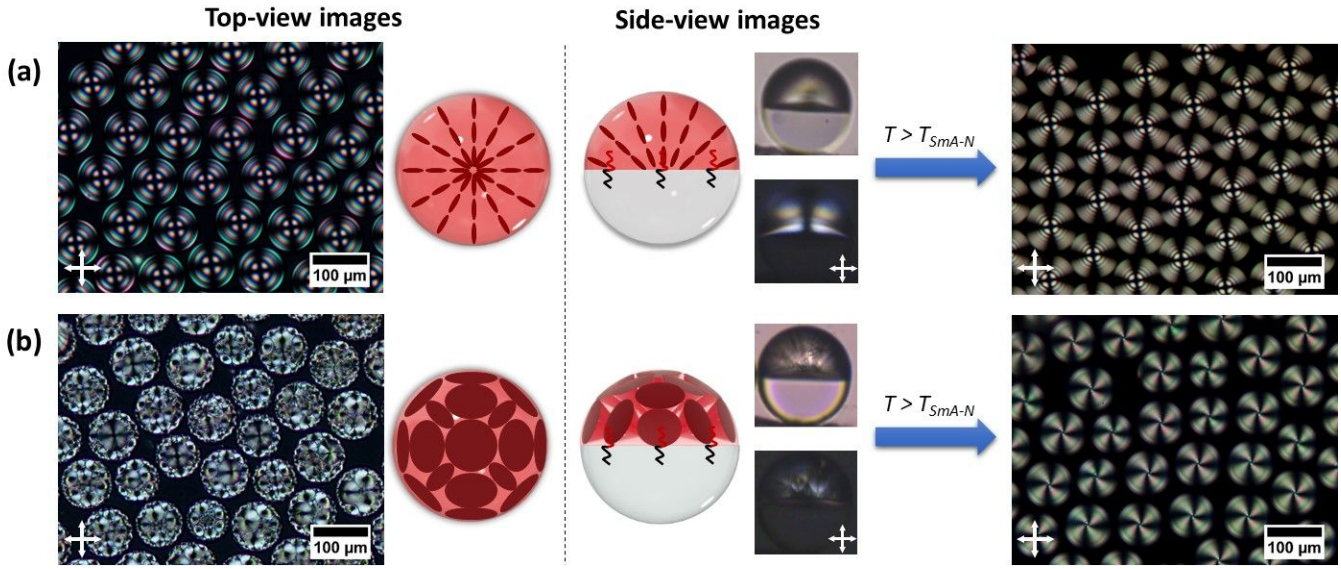

Figure 6. Smectic A LC complex emulsions: polarized-light optical microscopy images of 8CB-HFE7200 Janus droplets with **(a)** a radial alignment, and **(b)** planar alignment of the mesogens.

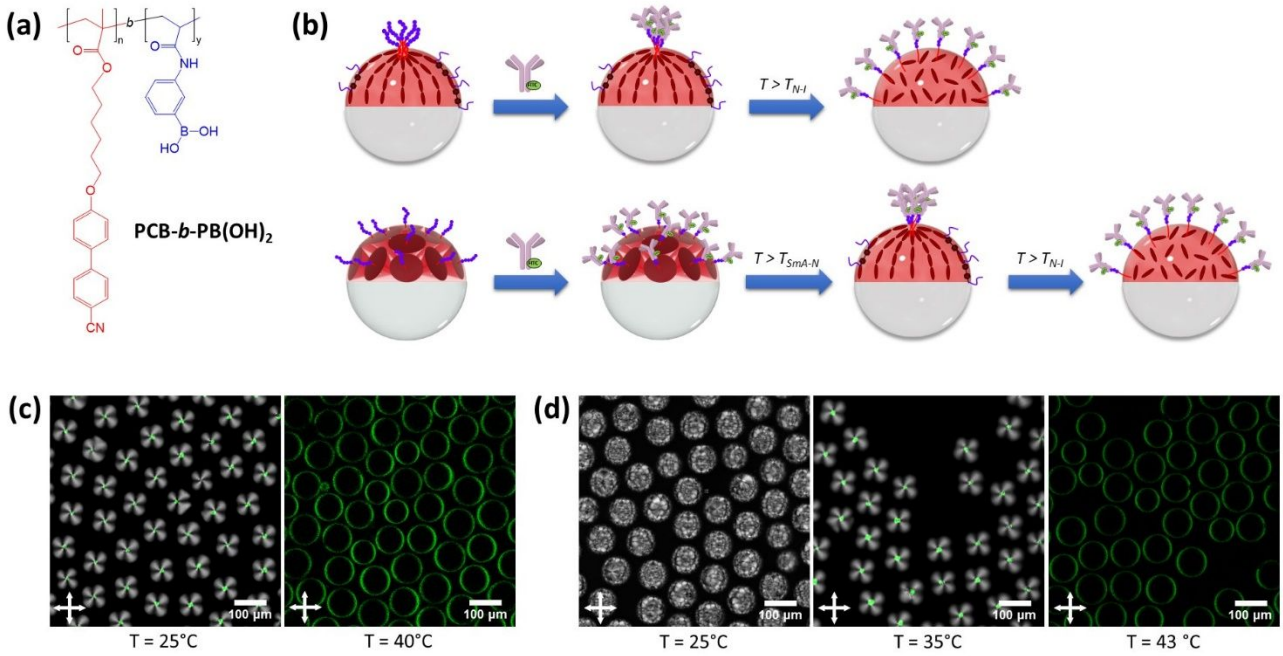

Figure 7. Antibody immobilization at topological defects: **(a)** Chemical structure of **PCB-*b*-PB(OH)$_2$**, the boronic acid block copolymer surfactant used for the functionalization of topological defects. **(b)** Schematic representation of the templated attachment of IgG antibodies at the point defect of nematic (top) and smectic A (down) complex emulsions using **PCB-*b*-PB(OH)$_2$**. **(c)** Confocal microscopy images of 5CB- and **(d)** 8CB-containing Janus droplets functionalized with a dye(FITC)-labeled IgG antibody at different temperatures.

PCB-*b*-PB(OH)$_2$ block copolymer was also used for bioconjugation of the 8CB spherical Janus droplets. However, no fluorescence was detected by confocal microscopy (Figure 7c), which is probably related to the presence of multiple focal-conic topological defects at the LC/W interface that distribute point emissive signals that are quenched or below the fluorescence detection limits. Functionalization was confirmed upon heating to the nematic phase (T > 33°C), where bright fluorescent was observed at the monopolar nematic topological defect (Figure 7c). Upon further heating to the isotropic state, fluorescence from the FITC-dye labeled IgG antibodies was observed throughout the LC/W interface, also

confirming a covalent attachment of IgG antibodies (Figure 7c).

CONCLUSIONS

Dynamically reconfigurable complex emulsions comprising two immiscible liquids, a liquid crystal and a fluorocarbon oil, were developed. The high intrinsic surface tension between the LC and the fluorocarbon phase gives a non-spherical, snowman morphology. Producing stable spherical LC droplets required the simultaneous balancing of all interfacial tensions, which was accomplished by the use of designed monomeric or polymeric internal surfactants. Once the interfaces were stabilized, spherical LC droplet morphologies could be dynamically switched between LC/F/W double emulsions, Janus emulsions, and inverted F/H/W double emulsions. The nematic LC stabilization developed for 5CB, can be extended to 8CB, a smectic A LC, creating droplets with more complex internal nanostructures. By using appropriately designed surfactants, we can create droplets with different LC director fields. In addition, by design LCs can be oriented in a radial direction (perpendicular to the interface) or in planar fashion (parallel to the interface). These designs were executed at both internal LC/F interfaces and the LC/W interface. The control of the position of the topological singularities allows for the precision assembly of antibodies. Dynamic complex colloids with controlled structures will provide access to a multitude of enticing sensing applications.

ASSOCIATED CONTENT

Supporting Information. Materials and Characterization Techniques; Experimental Procedures; Synthesis details and characterization of monomeric and polymeric surfactants. This material is available free of charge via the Internet at http://pubs.acs.org.

AUTHOR INFORMATION

Corresponding Author

* tswager@mit.edu

Notes

The authors declare no competing financial interest.

ACKNOWLEDGMENT

We are grateful for support from a Vannevar Bush Faculty Fellowship (Grant # N000141812878) from the Department of Defense. We also thank Samuel I. Etkind for mass spectrometry measurements.

REFERENCES

1. Aserin, A., *Multiple emulsion: technology and applications*. John Wiley & Sons: 2008.
2. Augustin, M. A.; Hemar, Y., Nano- and micro-structured assemblies for encapsulation of food ingredients. *Chem. Soc. Rev.* **2009,** *38* (4), 902-912.
3. McClements, D. J.; Li, Y., Structured emulsion-based delivery systems: Controlling the digestion and release of lipophilic food components. *Advances in Colloid and Interface Science* **2010,** *159* (2), 213-228.
4. Zhang, J.; Grzybowski, B. A.; Granick, S., Janus Particle Synthesis, Assembly, and Application. *Langmuir* **2017,** *33* (28), 6964-6977.
5. Forth, J.; Kim, P. Y.; Xie, G.; Liu, X.; Helms, B. A.; Russell, T. P., Building Reconfigurable Devices Using Complex Liquid–Fluid Interfaces. *Adv. Mater.* **2019,** *31* (18), 1806370.
6. Bijlard, A.-C.; Wald, S.; Crespy, D.; Taden, A.; Wurm, F. R.; Landfester, K., Functional Colloidal Stabilization. *Adv. Mater. Interfaces* **2017,** *4* (1), 1600443.
7. Yang, S.; Guo, F.; Kiraly, B.; Mao, X.; Lu, M.; Leong, K. W.; Huang, T. J., Microfluidic synthesis of multifunctional Janus particles for biomedical applications. *Lab on a Chip* **2012,** *12* (12), 2097-2102.
8. Choi, C.-H.; Kim, J.; Nam, J.-O.; Kang, S.-M.; Jeong, S.-G.; Lee, C.-S., Microfluidic Design of Complex Emulsions. *ChemPhysChem* **2014,** *15* (1), 21-29.
9. Zarzar, L. D.; Sresht, V.; Sletten, E. M.; Kalow, J. A.; Blankschtein, D.; Swager, T. M., Dynamically reconfigurable complex emulsions via tunable interfacial tensions. *Nature* **2015,** *518* (7540), 520-524.
10. Zhang, Q.; Savagatrup, S.; Kaplonek, P.; Seeberger, P. H.; Swager, T. M., Janus Emulsions for the Detection of Bacteria. *ACS Cent. Sci.* **2017,** *3* (4), 309-313.
11. Zeininger, L.; Nagelberg, S.; Harvey, K. S.; Savagatrup, S.; Herbert, M. B.; Yoshinaga, K.; Capobianco, J. A.; Kolle, M.; Swager, T. M., Rapid Detection of Salmonella enterica via Directional Emission from Carbohydrate-Functionalized Dynamic Double Emulsions. *ACS Central Science* **2019,** *5* (5), 789-795.
12. Zeininger, L.; Weyandt, E.; Savagatrup, S.; Harvey, K. S.; Zhang, Q.; Zhao, Y.; Swager, T. M., Waveguide-based chemo- and biosensors: complex emulsions for the detection of caffeine and proteins. *Lab on a Chip* **2019,** *19* (8), 1327-1331.
13. Zhang, Q.; Zeininger, L.; Sung, K.-J.; Miller, E. A.; Yoshinaga, K.; Sikes, H. D.; Swager, T. M., Emulsion Agglutination Assay for the Detection of Protein–Protein Interactions: An Optical Sensor for Zika Virus. *ACS Sensors* **2019,** *4* (1), 180-184.
14. Lin, C.-J.; Zeininger, L.; Savagatrup, S.; Swager, T. M., Morphology-Dependent Luminescence in Complex Liquid Colloids. *J. Am. Chem. Soc.* **2019,** *141* (9), 3802-3806.
15. Nagelberg, S.; Zarzar, L. D.; Nicolas, N.; Subramanian, K.; Kalow, J. A.; Sresht, V.; Blankschtein, D.; Barbastathis, G.; Kreysing, M.; Swager, T. M.; Kolle, M., Reconfigurable and responsive droplet-based compound micro-lenses. *Nat. Commun.* **2017,** *8*, 14673.
16. Tschierske, C., Development of Structural Complexity by Liquid-Crystal Self-assembly. *Angew. Chem. Int. Ed.* **2013,** *52* (34), 8828-8878.
17. van der Asdonk, P.; Kouwer, P. H. J., Liquid crystal templating as an approach to spatially and temporally organise soft matter. *Chem. Soc. Rev.* **2017,** *46* (19), 5935-5949.
18. Broer, D. J.; Bastiaansen, C. M. W.; Debije, M. G.; Schenning, A. P. H. J., Functional Organic Materials Based on Polymerized Liquid-Crystal Monomers: Supramolecular Hydrogen-Bonded Systems. *Angew. Chem. Int. Ed.* **2012,** *51* (29), 7102-7109.
19. Kato, T.; Uchida, J.; Ichikawa, T.; Sakamoto, T., Functional Liquid Crystals towards the Next Generation of Materials. *Angew. Chem. Int. Ed.* **2018,** *57* (16), 4355-4371.
20. Miller, D. S.; Wang, X.; Abbott, N. L., Design of Functional Materials Based on Liquid Crystalline Droplets. *Chem. Mater.* **2014,** *26* (1), 496-506.
21. Braun, L. B.; Zentel, R., Functional liquid crystalline particles and beyond. *Liq. Cryst.* **2019,** 1-19.

22. Brake, J. M.; Daschner, M. K.; Luk, Y.-Y.; Abbott, N. L., Biomolecular Interactions at Phospholipid-Decorated Surfaces of Liquid Crystals. *Science* **2003,** *302* (5653), 2094-2097.
23. Sivakumar, S.; Wark, K. L.; Gupta, J. K.; Abbott, N. L.; Caruso, F., Liquid Crystal Emulsions as the Basis of Biological Sensors for the Optical Detection of Bacteria and Viruses. *Adv. Funct. Mater.* **2009,** *19* (14), 2260-2265.
24. Lin, I.-H.; Miller, D. S.; Bertics, P. J.; Murphy, C. J.; de Pablo, J. J.; Abbott, N. L., Endotoxin-Induced Structural Transformations in Liquid Crystalline Droplets. *Science* **2011,** *332* (6035), 1297-1300.
25. Cipparrone, G.; Mazzulla, A.; Pane, A.; Hernandez, R. J.; Bartolino, R., Chiral Self-Assembled Solid Microspheres: A Novel Multifunctional Microphotonic Device. *Adv. Mater.* **2011,** *23* (48), 5773-5778.
26. Chen, L.; Li, Y.; Fan, J.; Bisoyi, H. K.; Weitz, D. A.; Li, Q., Photoresponsive Monodisperse Cholesteric Liquid Crystalline Microshells for Tunable Omnidirectional Lasing Enabled by a Visible Light-Driven Chiral Molecular Switch. *Advanced Optical Materials* **2014,** *2* (9), 845-848.
27. Kang, J.-H.; Kim, S.-H.; Fernandez-Nieves, A.; Reichmanis, E., Amplified Photon Upconversion by Photonic Shell of Cholesteric Liquid Crystals. *J. Am. Chem. Soc.* **2017,** *139* (16), 5708-5711.
28. Belmonte, A.; Bus, T.; Broer, D. J.; Schenning, A. P. H. J., Patterned Full-Color Reflective Coatings Based on Photonic Cholesteric Liquid-Crystalline Particles. *ACS Appl. Mater. Interfaces* **2019,** *11* (15), 14376-14382.
29. Schwartz, M.; Lenzini, G.; Geng, Y.; Rønne, P. B.; Ryan, P. Y. A.; Lagerwall, J. P. F., Cholesteric Liquid Crystal Shells as Enabling Material for Information-Rich Design and Architecture. *Adv. Mater.* **2018,** *30* (30), 1707382.
30. Ohm, C.; Serra, C.; Zentel, R., A Continuous Flow Synthesis of Micrometer-Sized Actuators from Liquid Crystalline Elastomers. *Adv. Mater.* **2009,** *21* (47), 4859-4862.
31. Fleischmann, E.-K.; Liang, H.-L.; Kapernaum, N.; Giesselmann, F.; Lagerwall, J.; Zentel, R., One-piece micropumps from liquid crystalline core-shell particles. *Nat. Commun.* **2012,** *3*, 1178.
32. Hessberger, T.; Braun, L. B.; Zentel, R., Interfacial Self-Assembly of Amphiphilic Dual Temperature Responsive Actuating Janus Particles. *Adv. Funct. Mater.* **2018,** *28* (21), 1800629.
33. Jampani, V. S. R.; Mulder, D. J.; De Sousa, K. R.; Gélébart, A.-H.; Lagerwall, J. P. F.; Schenning, A. P. H. J., Micrometer-Scale Porous Buckling Shell Actuators Based on Liquid Crystal Networks. *Adv. Funct. Mater.* **2018,** *28* (31), 1801209.
34. Jeong, J.; Gross, A.; Wei, W.-S.; Tu, F.; Lee, D.; Collings, P. J.; Yodh, A. G., Liquid crystal Janus emulsion droplets: preparation, tumbling, and swimming. *Soft Matter* **2015,** *11* (34), 6747-6754.
35. Wang, X.; Zhou, Y.; Kim, Y.-K.; Tsuei, M.; Yang, Y.; de Pablo, J. J.; Abbott, N. L., Thermally reconfigurable Janus droplets with nematic liquid crystalline and isotropic perfluorocarbon oil compartments. *Soft Matter* **2019,** *15* (12), 2580-2590.
36. Zhang, Q.; Liu, X.; Liu, D.; Gai, H., Ultra-small droplet generation via volatile component evaporation. *Lab on a Chip* **2014,** *14* (8), 1395-1400.
37. Zhang, Q.; Xu, M.; Liu, X.; Zhao, W.; Zong, C.; Yu, Y.; Wang, Q.; Gai, H., Fabrication of Janus droplets by evaporation driven liquid–liquid phase separation. *Chem. Commun.* **2016,** *52* (28), 5015-5018.
38. Guzowski, J.; Korczyk, P. M.; Jakiela, S.; Garstecki, P., The structure and stability of multiple micro-droplets. *Soft Matter* **2012,** *8* (27), 7269-7278.
39. Ge, L.; Friberg, S. E.; Guo, R., Recent studies of Janus emulsions prepared by one-step vibrational mixing. *Current Opinion in Colloid & Interface Science* **2016,** *25*, 58-66.
40. He, Y.; Savagatrup, S.; Zarzar, L. D.; Swager, T. M., Interfacial Polymerization on Dynamic Complex Colloids: Creating Stabilized Janus Droplets. *ACS Appl. Mater. Interfaces* **2017,** *9* (8), 7804-7811.
41. Eremin, A.; Nádasi, H.; Hirankittiwong, P.; Kiang-Ia, J.; Chattham, N.; Haba, O.; Yonetake, K.; Takezoe, H., Azodendrimers as a photoactive interface for liquid crystals. *Liq. Cryst.* **2018,** *45* (13-15), 2121-2131.
42. Gupta, J. K.; Zimmerman, J. S.; de Pablo, J. J.; Caruso, F.; Abbott, N. L., Characterization of Adsorbate-Induced Ordering Transitions of Liquid Crystals within Monodisperse Droplets. *Langmuir* **2009,** *25* (16), 9016-9024.
43. Kim, Y.-K.; Noh, J.; Nayani, K.; Abbott, N. L., Soft matter from liquid crystals. *Soft Matter* **2019,** *15* (35), 6913-6929.
44. Noh, J.; Henx, B.; Lagerwall, J. P. F., Taming Liquid Crystal Self-Assembly: The Multifaceted Response of Nematic and Smectic Shells to Polymerization. *Adv. Mater.* **2016,** *28* (46), 10170-10174.
45. Liang, H.-L.; Schymura, S.; Rudquist, P.; Lagerwall, J., Nematic-Smectic Transition under Confinement in Liquid Crystalline Colloidal Shells. *Phys. Rev. Lett.* **2011,** *106* (24), 247801.
46. Schenning, A.; Crawford, G. P.; Broer, D. J., *Liquid crystal sensors*. CRC Press, Taylor & Francis Group, CRC Press is an imprint of the Taylor & Francis Group, an informa business: Boca Raton, 2018; p xiv, 164 pages.
47. Wang, D.; Park, S.-Y.; Kang, I.-K., Liquid crystals: emerging materials for use in real-time detection applications. *J. Mater. Chem. C* **2015,** *3* (35), 9038-9047.
48. Škarabot, M.; Ravnik, M.; Žumer, S.; Tkalec, U.; Poberaj, I.; Babič, D.; Muševič, I., Hierarchical self-assembly of nematic colloidal superstructures. *Physical Review E* **2008,** *77* (6), 061706.
49. Mondiot, F.; Wang, X.; de Pablo, J. J.; Abbott, N. L., Liquid Crystal-Based Emulsions for Synthesis of Spherical and Non-Spherical Particles with Chemical Patches. *J. Am. Chem. Soc.* **2013,** *135* (27), 9972-9975.
50. Whitmer, J. K.; Wang, X.; Mondiot, F.; Miller, D. S.; Abbott, N. L.; de Pablo, J. J., Nematic-Field-Driven Positioning of Particles in Liquid Crystal Droplets. *Phys. Rev. Lett.* **2013,** *111* (22), 227801.
51. Wang, X.; Miller, D. S.; Bukusoglu, E.; de Pablo, J. J.; Abbott, N. L., Topological defects in liquid crystals as templates for molecular self-assembly. *Nature Mater.* **2015,** *15*, 106.

Table of Contents Artwork